Brazilian Journal of Physics
ISSN: 0103-9733
luizno.bjp@gmail.com
Sociedade Brasileira de Física
Brasil

Freitas, A. S.; Marques, L.; Zhang, X. X.; Luzio, M. A.; Guillaumon, P.; Pampa Condori, R.; Lichtenthaler, R.
Woods-Saxon Equivalent to a Double Folding Potential
Brazilian Journal of Physics, vol. 46, núm. 1, febrero, 2016, pp. 120-128
Sociedade Brasileira de Física
São Paulo, Brasil

Available in: http://www.redalyc.org/articulo.oa?id=46443233015

How to cite
Complete issue
More information about this article
Journal's homepage in redalyc.org

Scientific Information System
Network of Scientific Journals from Latin America, the Caribbean, Spain and Portugal
Non-profit academic project, developed under the open access initiative

Braz J Phys (2016) 46:120–128
DOI 10.1007/s13538-015-0387-y

SOCIEDADE BRASILEIRA DE FÍSICA

NUCLEAR PHYSICS

Woods-Saxon Equivalent to a Double Folding Potential

A. S. Freitas[1] · L. Marques[1] · X. X. Zhang[1] · M. A. Luzio[1] · P. Guillaumon[1] · R. Pampa Condori[1] · R. Lichtenthäler[1]

Received: 18 August 2015 / Published online: 17 November 2015
© Sociedade Brasileira de Física 2015

Abstract A Woods-Saxon equivalent to a double folding potential in the nuclear surface region is obtained for the heavy-ion scattering potential. The Woods-Saxon potential has fixed geometry and was used as a bare potential in the analysis of elastic scattering angular distributions of several stable systems. A new analytical formula for the position and height of the Coulomb barrier is presented, which reproduces the results obtained using double folding potentials. This simple formula has been applied to estimate the fusion cross section above the Coulomb barrier. A comparison with experimental data is presented.

Keywords Nuclear potential · Bare potential · Coulomb barrier · Elastic scattering · Fusion cross section

1 Introduction

The strong nuclear force is responsible for keeping the nucleons together inside the nucleus and is still not fully understood. The attractive force between the nucleons is the residuum of the interaction between quarks and gluons confined inside the nucleons, and the connection between the fundamental interaction and the nucleon-nucleon force is still an open problem. Elastic scattering between nuclei provides information of the strong nuclear interaction; however, the cross sections are affected by the couplings between the elastic scattering and all other possible reaction channels. As a consequence, the potential obtained from the analysis of elastic scattering angular distributions is the sum of a bare potential, which is real in principle, and a polarization term, which is complex and contains the effects of all couplings. To obtain information of the bare potential, only one should find a situation where the elastic is the only open channel. However, it is very difficult to find such experimental situation. Even at energies around the Coulomb barrier, where the reactions channels are closing, there is still the contribution of the fusion process, which makes the interacting potential complex. If one goes down to even lower energies, the effect of the short range nuclear potential becomes smaller and smaller as the long range Coulomb potential dominates and the scattering becomes pure Rutherford.

The nuclear bare potential can, in principle, be defined as the result of the double folding of the nucleon-nucleon interactions and the projectile and target nuclear densities [1–4]. The nucleon-nucleon interactions can be obtained from more fundamental theories. Double folding potentials have been used as the bare potential to analyse experimental data [5–7], and the imaginary part of the interaction is normally parameterized and freely searched to best fit the angular distributions. One of the most widely used parameterizations for the nuclear potential is the well-known Woods-Saxon (WS) shape [8], with three parameters that are adjusted to reproduce the data.

More recently, the São Paulo optical potential (SPP) has been developed, where the real part is taken as a double folding potential, and the imaginary part has the same geometry of the real part, with an additional fixed normalization factor. An energy dependence term is included to account for non-local corrections due to the Pauli principle [9]. The São Paulo potential has no free parameters and has been successfully applied to a large number of experimental angular distributions from low to intermediate energies [10–17].

✉ R. Lichtenthäler
rubens@if.usp.br

[1] Instituto de Física da Universidade de São Paulo, C.P. 66318, 05389-970, São Paulo, Brazil

Despite the success of the São Paulo potential in analysing elastic scattering data, it would be interesting to investigate the relation between the Woods-Saxon shape and the double folding potential. Most of the optical model and reaction programs use the WS parameterization whereas double folding potentials have to be entered externally from numerical files. The equivalence between WS and double folding potentials is not straightforward, and there is no WS that could reproduce the double folding shape in the whole radial range. However, heavy ion scattering at low energies is frequently sensitive only to the tail of the nuclear potential and not very much to the potential in the interior region, where strong absorption usually takes place.

In the present work, we determine the parameters of a WS potential that reproduce the real part of the double folding São Paulo potential in the surface region. We determine the geometry of this potential and apply it to experimental elastic scattering angular distributions of several systems.

Based on the real part of this potential, we found a simple analytical formula to obtain the position and the height of the Coulomb barrier which reproduces quite precisely the Coulomb barriers obtained from the São Paulo potential. This formulation is applied to estimate the fusion cross section in the region above the Coulomb barrier.

2 The Woods-Saxon Potential

The Woods-Saxon shape is given by:

$$f(r) = \frac{1}{1 + \exp(\frac{r-R}{a})} \tag{1}$$

where $R = r_0(A_1^{1/3} + A_2^{1/3})$ and a is the diffuseness. The optical potential is written as:

$$V_{nucl}(r) = -V_0 f_1(r) - i W_0 f_2(r) \tag{2}$$

where V_0 and W_0 are the real and imaginary strengths of the optical potential respectively and $f_i(r)$ are Woods-Saxon form factors that may have different values of radius and diffuseness parameters.

We developed a simple computer program to perform an automatic search on the three parameters V_0, r_0, a of (1) to reproduce the tail of the real part of the São Paulo potential for several systems.

The results are shown in Fig. 1 where the dashed lines represent the real part of São Paulo potential (SPP) calculated for several systems. The solid lines are the resulting Woods-Saxon potentials that best fit the SPP in the region $r > R$. We found that, for all systems analysed, the Woods-Saxon that best reproduces the tail of the SPP potential has a diffuseness $a \approx 0.65$ fm and $r_0 \approx 1.3$ fm for strengths ranging between $V_0 = 10 - 20$ MeV. In general, double folding potentials are strongly attractive with strengths of hundreds of MeV's.

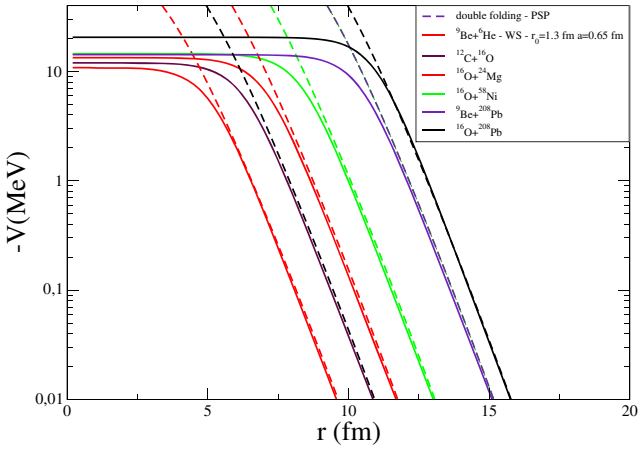

Fig. 1 Radial dependence of the real part of the nuclear potential for several systems

2.1 Ambiguities

Ambiguities in the optical potential have been the subject of many studies since the beginnings of nuclear physics [18]. The fact that the elastic scattering angular distributions in the strong absorption regime are sensitive to a small region in the surface of the nuclear potential has long been recognized. If the scattering at low energies is sensitive only to the tail of the nuclear potential, for a Woods-Saxon shape, one immediately gets that, for $(r - R) >> a$, one obtains $V_{nucl}(r) = -V_0 \exp(R/a) \exp(-r/a)$. Thus, for a given diffuseness a, any combination of V_0 and R that leaves $V_0 \exp(R/a)$ unchanged will provide the same potential in the surface region. In this sense, the parameters V_0 and r_0 proposed in the present paper are only one family of possible potentials.

3 The Coulomb Barrier

The height and position of the Coulomb barrier are very important parameters in the collision of two heavy ions. They basically determine the total reaction cross section at energies above the Coulomb barrier and can be obtained if the real part of the nuclear potential in the surface region is known.

The condition:

$$\frac{d}{dr}[V_{nucl}(r) + V_{coul}(r)]_{r=R_B} = 0 \tag{3}$$

determines the position R_B, and the height of the Coulomb barrier is given by $V_B = V_{nucl}(R_B) + V_{coul}(R_B)$. As usually

Table 1 Comparison between formulas (7) and (8) (WS) and the results for Coulomb barrier radius and height from numerical calculations using the double folding São Paulo potential (SPP)

		R_B(fm)		V_B(MeV)	
System	x	WS	SPP	WS	SPP
^{6}He+^{9}Be	51.45	7.63	8.00	1.22	1.32
^{12}C+^{16}O	13.06	7.92	8.15	7.66	7.78
^{16}O+^{24}Mg	8.24	8.40	8.55	14.84	14.85
^{16}O+^{58}Ni	4.94	9.35	9.40	31.99	31.68
^{9}Be+^{208}Pb	5.29	11.49	11.50	38.72	38.55
^{16}O+^{208}Pb	2.95	11.68	11.65	77.07	75.90
^{9}Be+^{27}Al	13.45	8.29	8.50	7.99	8.09
^{9}Be+^{64}Zn	8.35	9.28	9.37	17.01	17.01
^{9}Be+^{89}Y	7.44	9.81	9.93	21.12	21.07
^{9}Be+^{144}Sm	5.86	10.67	10.70	31.29	31.16

V_{nucl} is unknown, one may assume an approximate radius for the Coulomb barrier radius as:

$$\mathring{R}_B = R = r_0\left(A_1^{1/3} + A_2^{1/3}\right) \tag{4}$$

and use a simplified formula for the height of the Coulomb barrier:

$$\mathring{V}_B = \frac{Z_1 Z_2 e^2}{\mathring{R}_B} \tag{5}$$

In general, (4) and (5) do not yield very good results in comparison to Coulomb barriers obtained from realistic DF potentials. Equation (3) provides a position for the Coulomb barrier which is, in most cases, larger than the geometrical radius from (4). Indeed, one sees that, if one takes a Woods-Saxon form for the nuclear potential $V_{nucl}(r) = -V_0/[1 + \exp[(r-R)/a]]$ and $V_{coul}(r) = Z_1 Z_2 e^2/r$ in (3) one shows that, in the approximation $\exp((R_B - R)/a) >> 1$, the Coulomb barrier radius can be written as:

$$R_B = R + a\ln\left[\frac{R}{a} \times \frac{V_0}{\mathring{V}_B}\right] \tag{6}$$

This equation may not be exact but it displays the main physics of the relation between R and R_B. For a square potential ($a = 0$), one gets $R_B = R$ and there is no correction to R. As the diffuseness of the potential increases, the correction term in right hand side of (6) increases. Also, for larger Coulomb barriers, the correction decreases.

Taking $R = 1.3(A_1^{1/3} + A_2^{1/3})$ fm, $a = 0.65$ fm, $V_0 = 15$ MeV, and $\mathring{V}_B$ given by (5), one obtains:

$$R_B = R + 0.65\ln[x] \tag{7}$$

where $x = 27.1 \times \frac{(A_1^{1/3}+A_2^{1/3})^2}{Z_1 Z_2}$ is a positive dimensionless parameter. Note that the parameter x, which appears in the argument of the logarithm of the above equation, can also be written as $x = \exp((R_B - R)/a)$ and is larger than one in most cases as shown in Table 1.

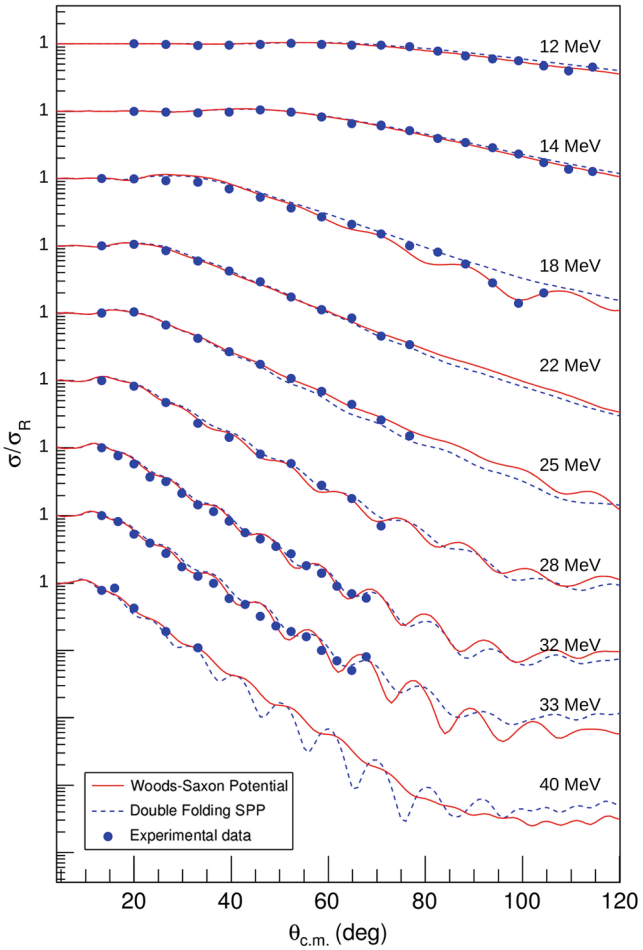

Fig. 2 Cross section for the ^{9}Be+^{27}Al system. The experimental data is from Ref. [22]. *Solid lines* are calculations with the WS potential and the *dashed lines* are calculations using SPP

Then one gets for V_B:

$$V_B = \frac{Z_1 Z_2 e^2}{R_B} - \frac{15}{x+1} \tag{8}$$

Table 2 Parameters of WS potential for the system ^{9}Be+^{27}Al

E_{lab} (MeV)	V_0 (MeV)	W_0 (MeV)	χ^2
12.0	18.15± 2.10	15.30± 7.68	0.36
14.0	15.22± 1.46	10.08± 2.90	0.47
18.0	17.87± 0.21	3.37± 0.17	4.35
22.0	16.45± 2.72	16.50± 4.05	0.69
25.0	12.22± 0.30	13.64± 0.01	1.83
28.0	17.39± 0.75	12.17± 0.52	3.92
32.0	15.90± 0.62	11.96± 0.52	6.24
33.0	17.43± 0.48	12.12± 0.35	13.36
40.0	8.29± 1.33	10.62± 1.85	2.70

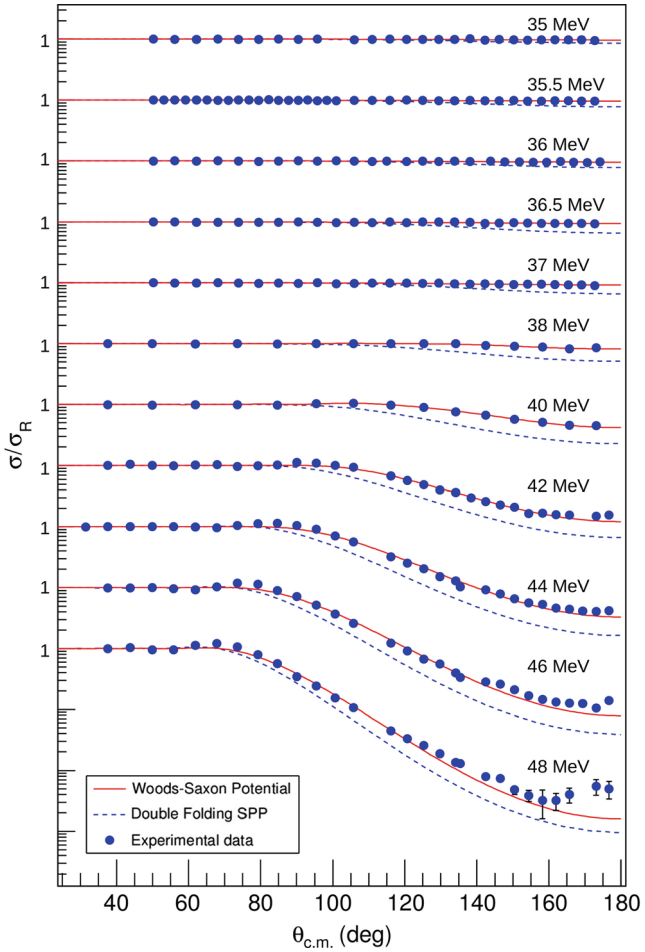

Fig. 3 Angular distributions for the ^{16}O+^{58}Ni system. *Solid lines* are calculations with the WS potential and the *dashed lines* are calculations using SPP

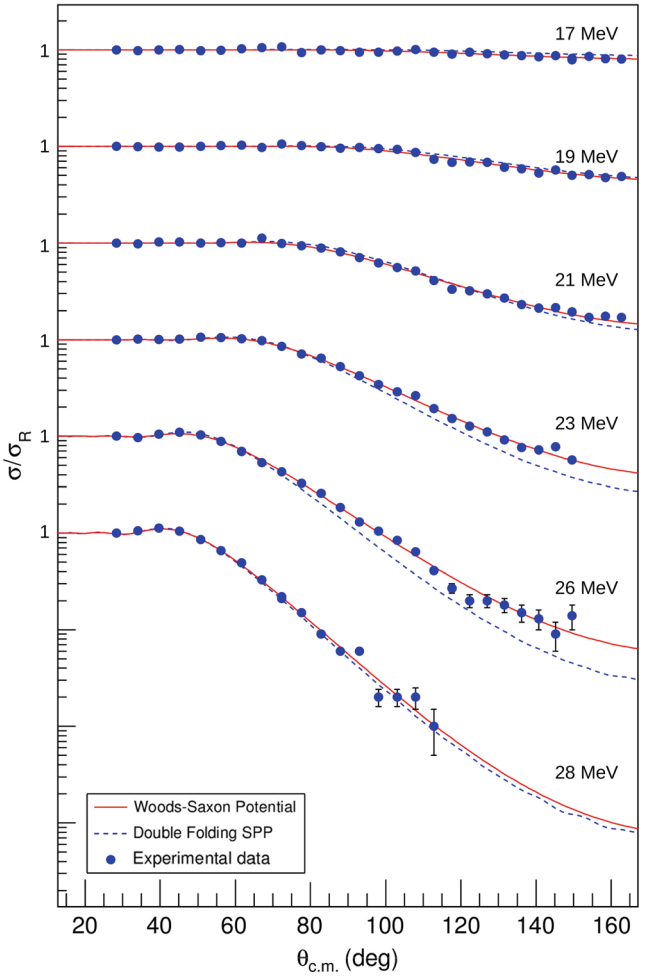

Fig. 4 Angular distributions for the ^{9}Be+^{64}Zn system. The experimental data is from Ref. [23]. *Solid lines* are calculations with the WS potential, and the *dashed lines* are calculations using SPP

Equations (7) and (8) depend only on the masses and charges of the nuclei and provide the Coulomb barrier position and height in very good agreement with those obtained from numerical calculations using the São Paulo Potential. This is shown in Table 1. The discrepancies are in the order of a few percent or smaller than that for heavier systems.

Table 3 Parameters of WS potential for the system ^{16}O+^{58}Ni

E_{lab} (MeV)	V_0 (MeV)	W_0 (MeV)	χ^2
35.0	$0.1^{+4.4}_{-0.1}$	3.8± 0.4	1.29
35.5	$0.1^{+1.5}_{-0.1}$	3.35± 0.27	1.24
36.0	$0.1^{+3.6}_{-0.1}$	3.54± 0.35	0.98
36.5	$2.6^{+4.4}_{-2.6}$	2.6± 0.8	2.01
37.0	$2.0^{+3.0}_{-2.0}$	3.5± 1.0	1.98
38.0	17.7± 0.3	0.15± 0.34	0.45
40.0	17.591± 0.002	1.18± 0.10	1.06
42.0	13.8± 0.4	5.29± 0.4	3.06
44.0	11.7888± 0.0006	7.6083± 0.0004	9.48
46.0	11.052± 0.007	9.677± 0.009	13.17
48.0	11.4212± 0.0002	11.1179± 0.0005	9.03

3.1 The curvature of the Coulomb barrier

One could go a step further and obtain the curvature of the Coulomb barrier based on the above potential. The region

Table 4 Parameters of WS potential for the system ^{9}Be+^{64}Zn

E_{lab} (MeV)	V_0 (MeV)	W_0 (MeV)	χ^2
17.0	$0.0^{+4.9}_{-0.0}$	36.21± 3.17	1.07
19.0	12.09± 1.43	19.17± 1.75	1.96
21.0	12.06± 0.29	18.88± 0.61	4.22
23.0	10.61± 0.16	14.51± 0.40	2.52
26.0	10.12± 0.18	15.98± 0.79	1.62
28.0	13.01± 0.25	12.47± 0.49	3.40

around the top of the Coulomb barrier can be approximated by an inverted harmonic oscillator potential of height V_B and frequency w. The frequency is related to V_B by:

$$\hbar w = \hbar\sqrt{(|d^2V(r)/dr^2|)_{r=R_B}/\mu} \tag{9}$$

where $V(r) = V_{nucl}(r) + V_{coul}(r)$, μ is the reduced mass and:

$$(d^2V(r)/dr^2)_{r=R_B} = -\frac{V_0}{a^2}\frac{x(x-1)}{(x+1)^3} + \frac{2Z_1Z_2e^2}{R_B^3} \tag{10}$$

Substituting $V_0 = 15$ MeV and $a = 0.65$ fm in the above formula, one can estimate the curvature of the Coulomb barrier.

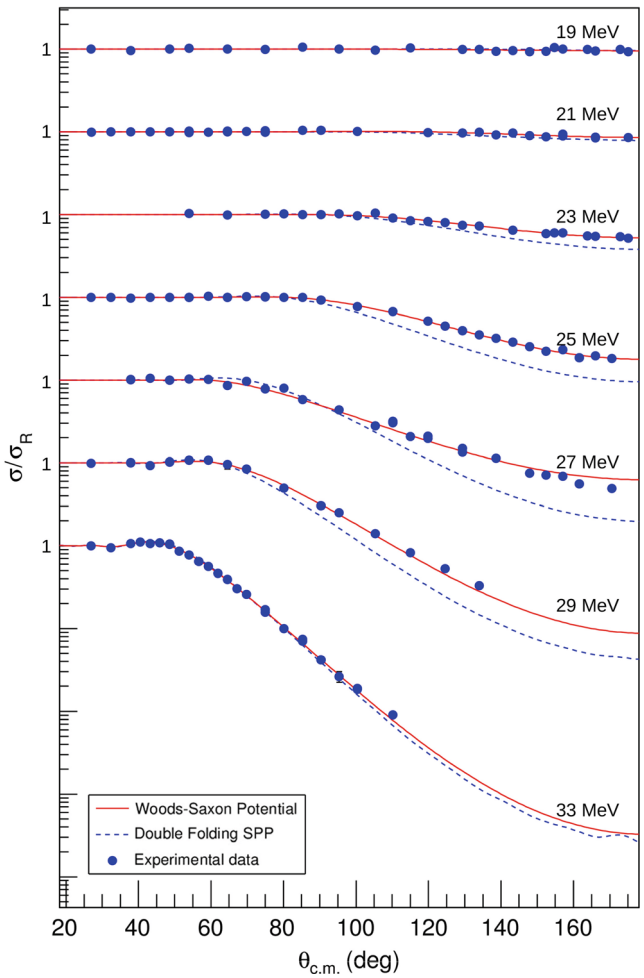

Fig. 5 Cross section for the ^{9}Be+^{89}Y system. The energy values are shown in Table 5. The experimental data are from Ref. [24]. *Solid lines* are calculations with the WS potential, and the *dashed lines* are calculations using SPP

4 Analysis of Experimental Data

In the next sections, we use this potential to analyse a number of experimental angular distributions. We fix the geometry of the real and imaginary parts to $r_0 = 1.3$ fm and $a = 0.65$ fm and allow V_0 and W_0 vary to best fit the angular distributions. The idea here is not to obtain excellent fits with such a simple potential but to show that it is possible to reproduce the general features of the angular distributions using this fixed geometry potential. For the sake of comparison, we analysed also all the angular distributions using the standard SPP with the usual normalization of the imaginary part $N_i = 0.78$.

All the optical model calculations have been performed using the program SFRESCO, the automatic search version of the FRESCO program [19]. The results are presented in the next subsections.

4.1 ^{9}Be+^{27}Al System

Nine elastic scattering ^{9}Be+^{27}Al angular distributions have been analysed [20] in the range from 12 MeV to 40 MeV in the laboratory system. Equation (8) gives $V_B = 10.65$ MeV for the Coulomb barrier energy in the laboratory system. The geometry of the real and imaginary potentials was fixed at $r_o = 1.3$ fm and $a = 0.65$ fm, and the depths V_0 and W_0 were varied to best fit the data. The Coulomb radius parameter was fixed at $r_{0c} = 1.3$ fm. The results are shown in Fig. 2, and the fitted parameters are presented in Table 2 together with the errors and the best reduced chi-square values. The errors have been estimated by the program SFRESCO using the gradient method used in the search procedure.

4.2 ^{16}O+^{58}Ni System

Eleven angular distributions from 35 to 48 MeV have been analysed [21]. $V_B^{cm} = 31.98$ MeV ($V_B^{lab} = 40.80$ MeV) for this system. The results are presented in Fig. 3 and in Table 3. The small values and large errors of V_0 shown in

Table 5 Parameters of WS potential for the system ^{9}Be+^{89}Y

E_{lab} (MeV)	V_0 (MeV)	W_0 (MeV)	χ^2
19.0	13.26± 0.40	17.37± 0.40	2.70
21.0	20.51± 0.92	1.36± 0.87	1.87
23.0	10.07± 0.68	7.48± 0.71	1.51
25.0	8.50± 0.01	7.93± 0.01	2.24
27.0	2.52± 0.34	29.12± 0.72	17.46
29.0	8.63± 0.16	11.59± 0.33	11.81
33.0	14.42± 0.10	15.11± 0.13	11.74

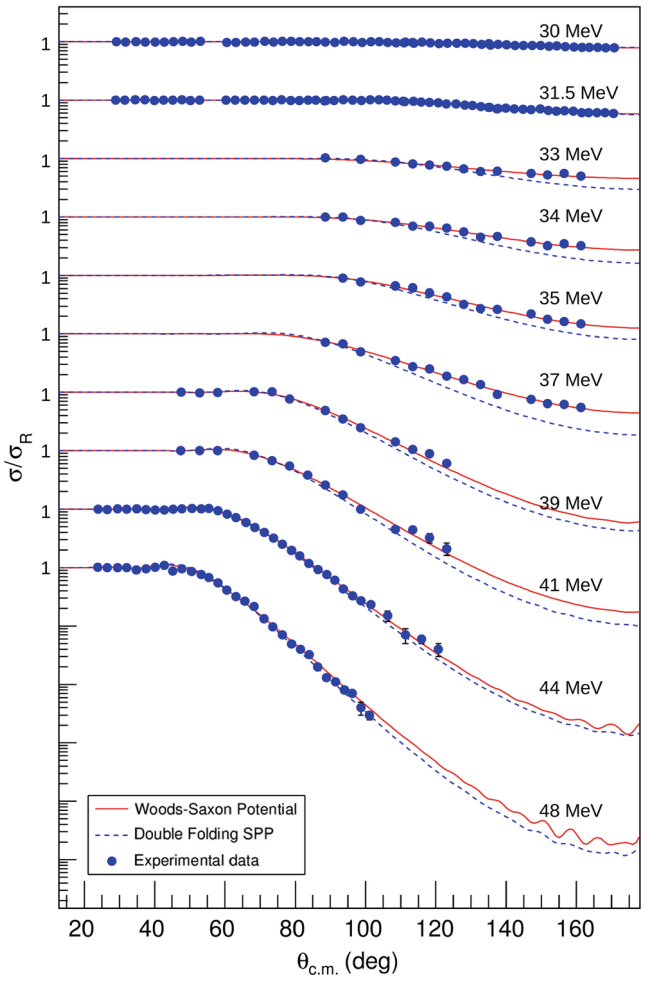

Fig. 6 Cross section for the ^{9}Be+^{144}Sm system. The energies values are shown in Table 6. The experimental data are from Ref. [22, 25]. *Solid lines* are calculations with the WS potential, and the *dashed lines* are calculations using SPP

Table 3 for $E_{lab} = 35 - 37$ MeV show that the potential is not determined at these energies below the Coulomb barrier.

Table 6 Parameters of WS potential for the system ^{9}Be+^{144}Sm

E_{lab} (MeV)	V_0 (MeV)	W_0 (MeV)	χ^2
30.0	11.99± 2.55	15.28± 1.09	1.16
31.5	13.94± 0.81	12.76± 0.57	1.32
33.0	$0.8^{+4.2}_{-0.8}$	16.76± 2.47	0.98
34.0	7.44± 1.59	13.03± 1.62	0.73
35.0	9.97± 0.83	13.41± 1.31	0.92
37.0	7.42± 0.58	17.00± 1.11	0.96
39.0	11.86± 0.42	13.41± 0.78	2.58
41.0	11.63± 0.45	15.81± 1.04	1.87
44.0	13.66± 0.18	15.67± 0.41	1.26
48.0	13.83± 0.16	16.86± 0.35	14.34

4.3 ^{9}Be+^{64}Zn System

Six angular distributions from 17 to 28 MeV in the laboratory system have been analysed [23]. The Coulomb barrier is at 19.4 MeV in the laboratory system (8), and the results are presented in Fig. 4 and the resulting parameters are in Table 4.

4.4 ^{9}Be+^{89}Y System

Seven angular distributions have been analysed for the ^{9}Be+^{89}Y system (Fig. 5). The laboratory energies range from 19 to 33 MeV and $V_B^{cm} = 21.11$ MeV ($V_B^{lab} = 23.25$ MeV). The results are presented in Table 5. The values of the imaginary part of the potential drop down to energies lower than the Coulomb barrier, except for the lowest energy.

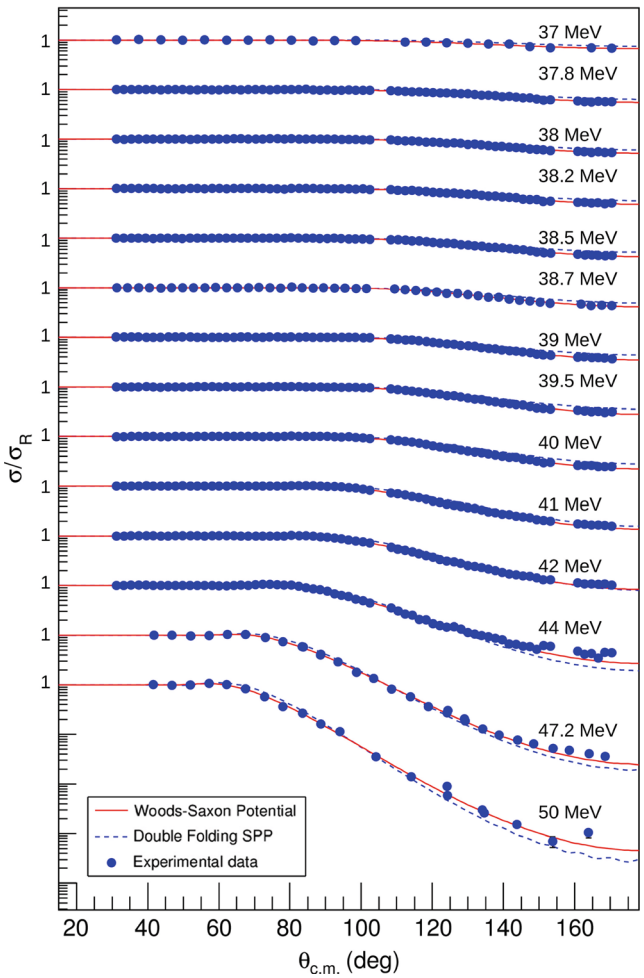

Fig. 7 Cross section for the ^{9}Be+^{208}Pb system. The parameters are shown in Table 7 and the experimental data are from Ref. [26]. The *dashed lines* are cross section from SPP

Table 7 Parameters of WS potential for the system ^{9}Be+^{208}Pb

E_{lab} (MeV)	V_0 (MeV)	W_0 (MeV)	χ^2
37.0	$0.1\ ^{+2.8}_{-0.1}$	29.38± 0.56	6.34
37.8	13.95± 0.84	21.58± 0.48	2.12
38.0	15.98± 0.64	19.98± 0.39	3.37
38.2	17.52± 0.54	18.69± 0.36	3.91
38.5	18.39± 0.37	18.53± 0.28	3.59
38.7	18.01± 0.53	17.27± 0.42	3.34
39.0	19.08± 0.25	17.18± 0.22	7.60
39.5	18.20± 0.20	17.79± 0.20	5.02
40.0	16.68± 0.18	19.06± 0.20	7.07
41.0	14.84± 0.07	19.76± 0.01	9.17
42.0	13.01± 0.10	20.69± 0.14	18.00
44.0	11.94± 0.19	20.89± 0.28	8.01
47.2	14.50± 0.07	19.84± 0.18	13.60
50.0	15.15± 0.11	22.81± 0.24	28.47

4.5 ^{9}Be+^{144}Sm System

Ten angular distributions for the ^{9}Be+^{144}Sm system have been analysed [22]. The energies range from below to above the Coulomb barrier at $V_B^{cm} = 31.28$ MeV ($V_B^{lab} = 33.24$ MeV). See Fig. 6 and Table 6.

4.6 ^{9}Be+^{208}Pb System

Fourteen angular distributions have been analysed in an energy around and below the Coulomb barrier [26]. $V_B^{cm} = 38.72$ MeV ($V_B^{lab} = 40.40$ MeV) for this system. See Fig. 7 and Table 7.

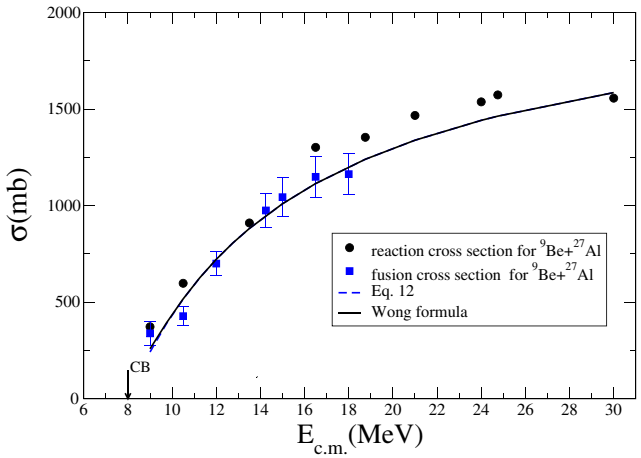

Fig. 8 Comparison between the total reaction, fusion cross section with predictions of formula (11) and (12) for the ^{9}Be+^{27}Al system with $R_B = 8.29$ fm, $V_B^{(cm)} = 7.99$ MeV and $\hbar w = 3.25$ MeV. The fusion cross sections were taken from ref. [28] and the reaction cross section are from the optical model calculations from Section 4.1

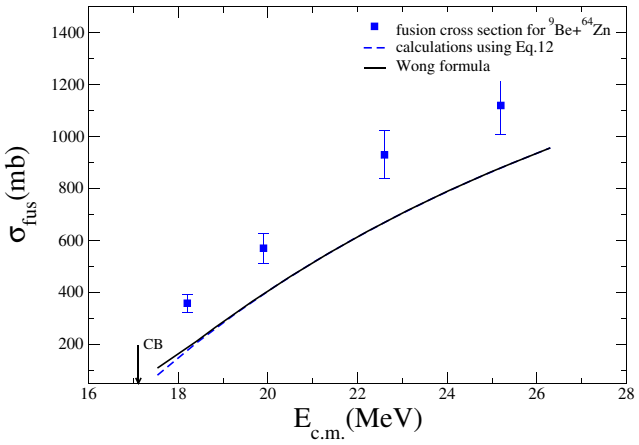

Fig. 9 Comparison between the total fusion cross section with predictions of formula (11) and (12) for the ^{9}Be+^{64}Zn system with $R_B = 9.28$ fm, $V_B^{(cm)} = 17.0$ MeV and $\hbar w = 3.44$ MeV. The fusion cross sections are taken from ref. [23]

5 Fusion and Total Reaction Cross Section

The total reaction cross section is an important information that can be obtained from the elastic scattering. In addition, at energies around the Coulomb barrier, in many cases, fusion exhausts most of the total reaction cross section and can be estimated by barrier penetration calculations. The well known Wong formula [27] for fusion has been applied with success to provide estimations of the fusion cross section.

$$\sigma_{wong} = \frac{R_B^2 \hbar w}{2E_{c.m.}} \ln\{1 + \exp[2\pi(E - V_B)/\hbar w]\} \qquad (11)$$

This formula depends on three parameters, the Coulomb barrier position, height and its curvature ($\hbar w$), the same

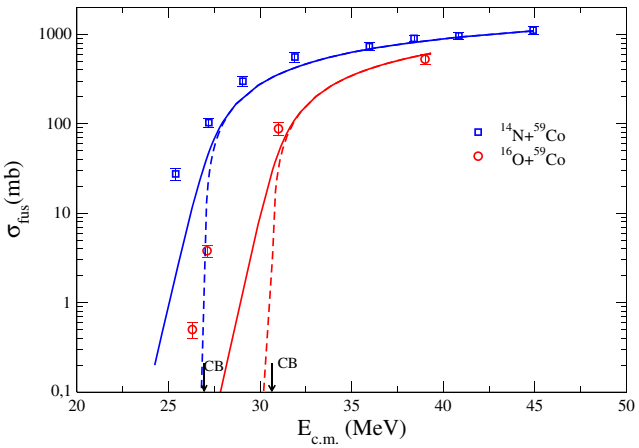

Fig. 10 Comparison between the total fusion cross section with predictions of formula (11) and (12) for the ^{14}N+^{59}Co and ^{16}O+^{59}Co systems. The fusion cross sections are taken from ref. [25]

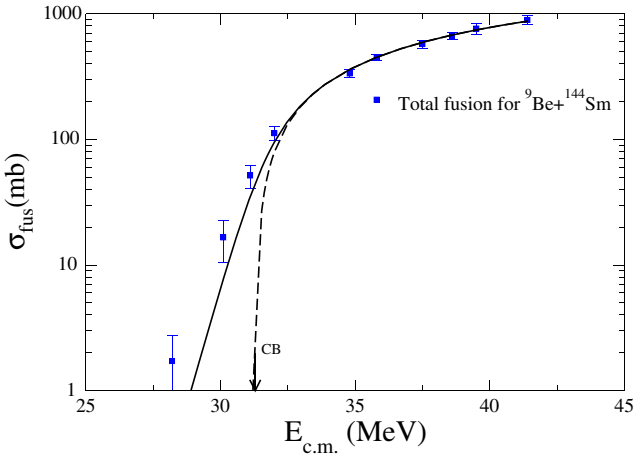

Fig. 11 Comparison between the total fusion cross section with predictions of formula (11) and (12) for the ^{9}Be+^{144}Sm system [29]. $R_B = 10.67$ fm, $V_B^{(cm)} = 31.29$ MeV and $\hbar w = 3.54$ MeV. The fusion cross sections are taken from ref. [29]

parameters that have been determined on Section 3. For energies above the Coulomb barrier, the Wong formula reduces to a simpler one which depends only on two parameters, the position and height of the Coulomb barrier.

$$\sigma = \pi R_B^2 (1 - \frac{V_B}{E}) \tag{12}$$

We applied formulas (11) and (12) using the parameter calculated from formulas (7), (8), (9) and (10) for the ^{9}Be+^{27}Al, ^{9}Be+^{64}Zn, ^{14}Ni+^{59}Co, ^{16}O+^{59}Co, ^{9}Be+^{144}Sm, and ^{16}O+^{208}Pb systems. The results are shown in Figs. 8, 9, 10, 11, and 12.

We see that formulas (11) (solid) and (12) (dashed) give the same result as the energy overcomes the Coulomb barrier. The agreement between the experimental fusion cross section and calculation is reasonable for energies above the Coulomb barrier. For energies below the barrier the calculations predict a cross section much smaller than the experimental one as can be seen in Fig. 10. This is expected since it is well known that for energies below the Coulomb barrier the fusion is strongly affected by coupled channels effects, which are obviously not taken into account by the simple formulation presented here.

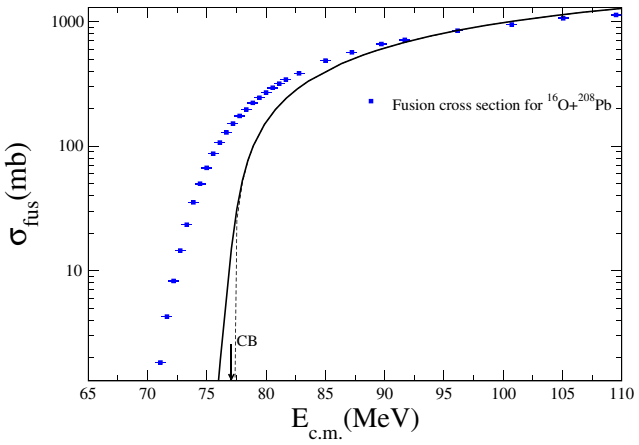

Fig. 12 Comparison between ^{16}O+^{208}Pb fusion cross sections [30] and the calculations using the Wong formula and $R_B = 11.68$ fm, $V_B^{(cm)} = 77.07$ MeV and $\hbar w = 2.45$ MeV

6 Conclusions

The real part of a Woods-Saxon potential that fits a double folding potential in the surface region ($r > R$) has been obtained. It was found that the tail of the double folding potential can be very well reproduced in all cases analysed here using a Woods-Saxon potential with a fixed geometry $r_0 = 1.3$ fm and $a = 0.65$ fm and depths varying between 10 and 20 MeV. There is a continuum ambiguity between r_0 and V_0.

A simple analytical formula has been derived using the real potential with depth $V_0 = 15$ MeV, which provides the position and height of the Coulomb barrier in very good agreement with the double folding potential predictions. It is shown that the Coulomb barrier position and height depend on a single dimensionless parameter x, which can be easily calculated as a function of the masses and charges of the colliding nuclei.

An optical model analysis has been performed for several systems using such potential, fixing the geometry for the real and imaginary parts, and adjusting the depths V and W to fit the angular distributions. It is shown that the potential proposed here provides reasonable fits of the scattering angular distributions for several stable systems at several energies above and below the Coulomb barrier. A strong variation of V_0 and W is observed at energies around the Coulomb barrier, as expected, due to the closing of the reaction channels as the energy goes down below the Coulomb barrier.

A criticism could be done to the optical model analysis presented here since the obtained potentials are not anymore strictly equivalent to the double folding, not even in the surface region, because of the free variation of the real and imaginary depths. This is true and it must be indeed just like that since the optical potentials that reproduce the data are not anymore the bare potential but the total optical potential, which includes all the polarization effects from the couplings with other reaction channels.

Total reaction and fusion cross sections have been calculated using the analytical formula derived here, and the result is compared with experimental fusion cross sections.

It is shown that, above the Coulomb barrier, the analytical formula provides a good approximation for the fusion cross sections and the calculations can be done with a simple pocket calculator without the need of numerical computations.

Acknowledgments authors wish to thank the Fundação de Amparo à Pesquisa do Estado de São Paulo (FAPESP) and the Conselho Nacional de Desenvolvimento Científico e Tecnológico (CNPq), Coordenação de Aperfeiçoamento de Pessoal de Nível Superior (CAPES) and Comissão Nacional de Energia Nuclear (CNEN) for financial support.

References

1. G.R. Satchler, Phys. Lett. **59B**, 121 (1975)
2. G.R. Satchler, W.G. Love, Phys. Lett. **65B**, 415 (1976)
3. W.G. Love, Phys. Lett. **72B**, 4 (1977)
4. G. Bertsch, Nucl. Phys. **A284**, 399 (1976)
5. P. Mohr, et al., Phys. Rev. **C 82**, 047601 (2010)
6. J.R.B. Oliveira, et al., EPJ. Web of Conferences **2**, 02002 (2010)
7. A. Gomez Camacho, P.S.R. Gomes, J. Lubian, J. Phys.: Conf. Ser. **322**, 012008 (2011)
8. R.D. Woods, D.S. Saxon, Phys. Rev. **95**(2), 577 (1954)
9. L.C. Chamon, D. Pereira, M.S. Hussein, M.A. Candido Ribeiro, D. Galetti, Phys. Rev. Lett. **79**, 5218 (1997)
10. L.R. Gasques, L.C. Chamon, C.P. Silva, D. Pereira, M.A.G. Alvarez, E.S. Rossi Jr., V.P. Likhachev, B.V. Carlson, C. De Conti, Phys. Rev. C **65**, 044314 (2002)
11. L.C. Chamon, et al., Phys. Rev. **C66**, 014610 (2002)
12. L.R. Gasques, L.C. Chamon, D. Pereira, et al., Phys. Rev. **C67**, 024602 (2003)
13. M.A.G. Alvarez, L.C. Chamon, M.S. Hussein, D. Pereira, L.R. Gasques, E.S. Rossi Jr., C.P. Silva, Nucl. Phys. **A723**, 93 (2003)
14. L.R. Gasques, A.V. Afanasjev, E.F. Aguilera, et al., Phys. Rev. C **72**, 025806 (2005)
15. J.M. Figueira, D. Abriola, J.O. Niello, et al., Phys. Rev. C **73**, 054603 (2006)
16. E.A. Benjamin, A. Lepine-Szily, D.R. Mendes Jr., et al., Phys. Lett. B **647**, 30 (2007)
17. L.F. Canto, P.R.S. Gomes, J. Lubian, et al., Nucl. Phys. A **821**, 51 (2009)
18. G. Igo, Phys. Rev. **115**, 1665 (1959)
19. I.J. Thompson, Comp. Phys. Rep. **7**, 167 (1988)
20. P.R.S. Gomes, et al., Phys. Rev. C **70**, 054605 (2004)
21. L.C. Chamon, et al., Nucl. Phys. **A597**, 253 (1996)
22. P.R.S. Gomes, et al., Phys. Rev. C **73**, 064606 (2006)
23. S.B. Moraes, et al., Phys. Rev. C **61**, 064608 (2000)
24. C.S. Palshetkar, et al., EPJ. Web of Conferences **17**, 03006 (2011)
25. P.R.S. Gomes, et al., Nucl. Phys. **A534**, 429 (1991)
26. N. Yu, et al., J. Phys. G. **37**, 075108 (2010)
27. C.Y. Wong, Phys. Rev. Lett. **31**, 766 (1973)
28. G.V. Martí, et al., Phys. Rev. **C71**, 027602 (2005)
29. P.R.S. Gomes, et al., Nucl. Phys. **A828**, 233 (2009)
30. C.R. Morton, et al., Phys. Rev. **C60**, 044608 (1999)